On the transitions in quasi-brittle failure of disordered solids

Ashwij Mayya

On the transitions in quasi-brittle failure of disordered solids

Ashwij Mayya*
Institut Jean Le Rond D'Alembert UMR 7190, Sorbonne Université, CNRS, Paris, France
(Dated: January 10, 2023)

The intermittent damage evolution preceding the failure of heterogeneous solids is well-described by robust scaling relations. Origin of such statistics is often attributed to the strength of material disorder. Yet, the acoustic emissions during failure of weakly disordered solids also exhibit robust scale-free statistics. Here, we numerically examine the precursory damage evolution considering an additional parameter, the damage hardening of the mesoscopic elements to interpret the microfracturing processes at lower length-scales. Interestingly, it allows a critical interpretation of precursory damage activity even for a case of weak disorder. We then derive a quasi-brittleness phase diagram showing that brittle and ductile-like failure of heterogeneous solids belong to different universality classes, reminiscent of the percolation and the depinning transitions. Our findings shed light on the range of Omori law exponents reported in literature as corresponding to the brittleness of the damaging solid.

Failure of heterogeneous solids advances through intermittent bursts of localized damage activity (e.g., microcracks) that are in interaction [1–3]. The acoustic emissions accompanying the precursory damage activity display remarkably robust scaling relations and present a progressively coherent spatial and temporal distribution of events that finally localize along a plane at failure [4, 5]. They assert the collective nature of damage growth in heterogeneous solids. And yet apart from the presence of power laws, insights on the characteristic aspects of damage spreading remain elusive. Consequently, the connection of precursors with failure is also ill-defined.

Motivated by the scale-free statistics of failure precursors and their divergence on approaching failure, a critical phenomenon scenario for the failure of heterogeneous solids is proposed [6–11]. In support, the exponent τ_{ae} characterizing the distribution of the energies of the acoustic emissions, $P(E_{ae}) \sim E_{ae}^{-\tau_{ae}}$ is reported to be $1.3 - 1.5$ during experiments on a wide class of materials [6–17]. Their frequency close to failure is also a power-law, $dN_{ae}/dt \sim |t_c - t|^{-\alpha_N}$ [18]. The value of exponent α_N is however dependent on material: $0.5 - 0.75$ for specimens of synthetic SiO_2 and rocks [11, 12, 15], concrete [16], and ~ 1.0 for shale [14] and teeth [17] during the experiments of compressive failure. Higher values of the exponent are reported during the non-compressive failure modes : 1.4 for un-notched specimens of paper during uniaxial tension tests [10], 1.68 and 1.28, respectively for specimens of bamboo chopsticks [13] and marble [19] during three-point bending tests. Such a wide range is in stark contrast with the expectations of an *universal* exponent, a hall-mark of critical phenomenon. Independent of the experiments, several numerical models that consider the collective nature of damage growth propose a discontinuous transition during failure [20–22]. The seemingly critical aspects of precursors are argued as emerging from the sweeping of an instability. Only for the case of strong disorder, failure is described as a smooth transition of the percolation type [23–26].

As a means to resolve these evidently contrasting interpretations, we recently proposed an unifying framework of damage evolution during compressive failure of disordered solids borrowing concepts from continuum damage mechanics and out-of-equilibrium physics of disordered systems [27, 28]. We show the precursory damage bursts as reminiscent of the depinning dynamics of a driven elastic interface [29, 30] that approaches an instability. Such an interpretation provided numerous time-to-failure scaling laws for precursors to be used as early warning signals [31]. However, the role of damage hardening, a subtle but an important aspect of the framework that controls the progressive damage accumulation at the mesoscopic level was not examined. As experiments with a relatively short damage accumulation phase *e.g.,* failure during tension, bending etc. may have minimal damage hardening, understanding the influence of hardening becomes essential for a broader relevance of our results.

In this letter, we numerically examine the roles of disorder and damage hardening during the failure of heterogeneous solids. Notably, at odds with the findings of a disorder dependent quasi-brittle failure of heterogeneous solids in literature [22, 25, 26, 32], we obtain scale-free statistics for precursors even for a weakly-disordered solid with moderate damage hardening. One of our crucial findings is that tuning the hardening above a threshold manifests a brittle to ductile-like transition in failure with their precursory activity corresponding to two different universality classes. When hardening is nearly absent, a percolation-like transition is observed. Whereas at large hardening, the precursors resemble depinning avalanches. Interestingly, this transition also manifests as a larger exponent in the power-law scaling of the dissipated energy rate as the failure is approached. Our findings provide a rationalization for the wide-range of exponents for the Omori law reported in literature and suggest that it describes the brittleness index of the heterogeneous solid.

Theoretical description: We will briefly present the theoretical framework for elasto-damageable solids that

is encoded in the numerical modeling. The detailed explanation of the approach is presented elsewhere [27, 28]. We obtain a mesoscopic description of both the damage field and the elastic interactions by interpreting the microfracturing processes at lower length-scales as a gradual increase in local damage level $d(\vec{x},t)$ at the location $\vec{x}$ and time t. The applied stress by the test machine is $\sigma_\circ(t)$. To deduce the damage growth at $(\vec{x},t)$, we use an energy criterion involving (i) a loading dependent local driving force $Y[d(\vec{x},t),\sigma_\circ]$ which provides the rate of elastic energy released for an incremental growth of damage and (ii) local damage resistance $Y_c[d(\vec{x},t)]$ which provides the material resistance to damage and corresponds to the rate of energy dissipated for an incremental growth of damage [33, 34]. The damage criterion then writes as

$$\begin{aligned} &Y[d(\vec{x},t),\sigma_\circ] < Y_c[d(\vec{x},t)] \rightarrow \text{stable damage,} \\ &Y[d(\vec{x},t),\sigma_\circ] = Y_c[d(\vec{x},t)] \rightarrow \text{damage grows.} \end{aligned} \tag{1}$$

To track the damage evolution, first we consider an initial reference damage level $d_\circ(0)$ at which the driving force and the damage resistance are $Y_\circ[d_\circ,\sigma_\circ]$ and $Y_{c\circ}(d_\circ)$, respectively. We then focus on the evolution of the perturbations that writes as $\Delta\dot{d}(\vec{x},t) \propto \Delta Y[\Delta d(\vec{x},t),\sigma_\circ] - \Delta Y_c[\Delta d(\vec{x},t)]$ assuming an over-damped dynamics. The right hand side of this relation describing the generalized driving force for damage growth can be organized in three terms as

$$\begin{aligned} \Delta\dot{d}(\vec{x},t) \propto &\mathcal{K}(\sigma_\circ)\,[v_m(\sigma_\circ)\,t - \Delta d(\vec{x},t)] + \\ &\psi(\sigma_\circ) * [\Delta d(\vec{x},t) - \langle \Delta d\rangle_{\vec{x}}] - y_c[\vec{x}, d(\vec{x},t)] \end{aligned} \tag{2}$$

Here $\mathcal{K}(\sigma_\circ) = \frac{\partial(Y_{c\circ} - Y_\circ)}{\partial d_\circ}$ describes the stability of damage evolution and $v_m(\sigma_\circ) \sim 1/\mathcal{K}$ provides the dissipation rate during damage spreading. The second (non-local) term of Eq.(4) describes the long-range interactions in the damage field taking values based on the perturbations $\Delta d(\vec{x},t)$. In principle, the kernel $\psi(\sigma_\circ)$ also describes the driving force redistribution in $\vec{x} \neq \vec{x}_0$ following the incremental damage growth at $\vec{x} = \vec{x}_0$. For the case of 2D, $\psi(\sigma_\circ) \sim 1/r^2$ where r is the radial distance from the damage event [35]. The last term in the equation represents the effect of material disorder. The resemblance of Eq. (4) to the equation of motion of driven disordered elastic interfaces [30, 36] allows for a robust interpretation of the precursory activity as avalanches during the depinning of a driven pseudo-interface (damage level) over a disordered field of damage resistance, even as the stability of the damage evolution progressively deteriorates [27, 28].

Damage hardening: In Eq. (4), we note that ensuring stable damage growth $\mathcal{K} > 0$ necessitates the value of the damage resistance to increase with the damage level. We assume a linear relation $Y_{c\circ}(d_\circ) = Y_c^\circ(1 + \eta d_\circ)$ where Y_c° is the characteristic damage resistance and η is the hardening coefficient. As a result, the first term of $\mathcal{K}(\sigma_\circ) = \frac{\partial(Y_{c\circ} - Y_\circ)}{\partial d_\circ}$ is a constant $Y_c^\circ\,\eta$. With increasing driving, the second term $\frac{\partial Y_\circ}{\partial d_\circ}$ increases, finally equaling $\frac{\partial Y_{c\circ}}{\partial d_\circ} = Y_c^\circ\,\eta$ at failure. Thus, damage hardening inferred at the mesoscopic scale describes both the approach to failure and the critical stress at failure. We infer the hardening to result from the material elements expending through their distribution of microfracturing thresholds, starting from the lowest values. Such a hierarchical description effectively bridges the conventional models such as global load sharing fiber-bundle to the damage spreading at the continuum level. Progressive damage growth at the local scale is often considered in literature [32, 37–42]. We note the damage hardening may be dependent on the both the type of material and the loading conditions. Unlike compressive failure where the stress concentration at tips of the microcracks is countered by the remotely applied stress leading to damage hardening [37, 38, 43–48], tensile failure often has a shorter damage accumulation phase where stress concentrations from one of the microcracks may trigger catastrophic failure. Even in case of compressive failure, increasing hardening was shown to change the nature of microcracking processes: from tensile to shear cracks in crystalline rocks [49, 50], from dilatant failure to compaction shear banding in porous rocks [51], from microcracking to plasticity in silicate rocks [52]. In the following, we examine the role of damage hardening at a fixed value of Y_c° and by varying the hardening coefficient η.

Numerical implementation: We numerically solve the evolution equation (4) as a feedback mechanism involving material disorder and elastic interactions [35]. We obtain bursts of damage at fixed stress as cascades. We follow the procedure of Berthier *et al.* [27] and consider a grid of size $L = 51$ discretized into L^2 elements with periodic boundary conditions. We use the kernel derived for the case of uni-axial compression [28]. The variation of elastic modulus with increasing damage is given by $E_\circ = E^\circ(1 - d_\circ^2)$ with $E^\circ = 1.01$MPa. We consider the disorder in the damage resistance field as being described by Gaussian distribution $\mathcal{N}(0,\beta)$. The characteristic damage resistance in the hardening rule is taken as $Y_c^\circ = 1.4$ kJ/m^3. The incremental damage $\delta d_\circ$ is 0.005.

The typical stress-strain response from the simulations is shown in Fig. 1(a). Beyond an elastic limit σ_{el}, the constitutive response comprises a sequence of force plateaus (see inset of Fig. 1(a)) and elastic loading segments. Damage evolution manifests as micro-instabilities that are stabilized by the redistribution of elastic energy. However, at critical stress σ_c, the damage grows unstably resulting in catastrophic failure. The value of stress corresponding to macroscopic instability is strongly influenced by the material disorder when the damage hardening is nearly absent as shown in Fig. 1(b). It also ensures a larger strain at failure, see inset of Fig. 1(b), in good agreement with Kumar *et al.* [32]. Interestingly, when

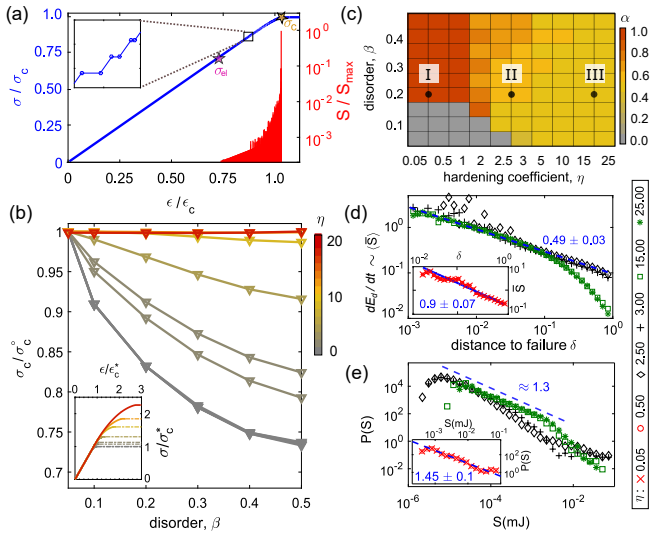

FIG. 1. (a) Typical stress-strain response (in blue) from the damage model with the hardening coefficient $\eta = 2.5$ and disorder $\beta = 0.2$ that is normalized by the values at failure. Inset: damage cascade manifests at microscopic scale as a force plateau. The size of precursors S normalized by the maximum value $S/S_{\max}$ (in red) is shown to increase on approaching failure. (b) Variation of normalized critical stress σ_c/σ_c° with varying disorder and hardening coefficient where σ_c° is the the value for the case of disorder $\beta = 0.05$. Inset: Effect of hardening on the stress-strain response for a fixed disorder $\beta = 0.2$. σ_c^* and ϵ_c^* are the failure stress and failure strain for the case $\eta = 0.05$. (c) The values of the exponent α, characterizing the power-law divergence of dissipation rate dE_d/dt on approaching failure for different values of disorder and hardening (line color). Note that the abscissa axis is non-uniform. (d) The divergence of the average size of the precursors normalized by the median value, $\langle S\rangle$ with distance to failure δ and (e) The distribution of the size of the precursors S for typical data-sets from zones II and III and zone I (in the inset).

damage hardening is prominent, the effect of material disorder on the strength is offset, thereby emphasizing the relevance of this study. We will now focus on the failure precursors. In Fig. 1(a), we find the damage cascades increasing in size on approaching failure. This is reminiscent of the acoustic emission accompanying damage growth in complex structural materials described in the introduction. To contextualize their evolution, we define the distance to failure $\delta = (\sigma_c - \sigma_\circ)/(\sigma_c - \sigma_{\rm el})$. We then obtain the dissipation rate diverging as a power-law on approaching failure $dE_d/dt \propto \delta^{-\alpha}$ as shown in Fig. 1(c) and (d). Interestingly, as the activity rate for the damage cascades was a constant, we observe $dE_d/dt \sim \langle S\rangle$. Determining the range of exponent α for varying disorder and hardening coefficient, we then find a phase-diagram like organization of quasi-brittleness as shown in Fig. 1(c). We infer a case of brittle failure for weak disorder and insignificant hardening (near the origin) as very few precursors are recorded. Increasing the strength of disorder results in quasi-brittle failure, an observation that matches with the reported literature [22, 25, 26]. The value of the exponent $\alpha \sim 0.9$. We now examine the role of damage hardening. In presence of moderate hardening, we obtain a smaller value of exponent $\alpha \sim 0.5$ even for the case of weak disorder (e.g. $\beta \simeq 0.05, \eta \simeq 5.0$). Increase in hardening still provides $\alpha \sim 0.5$. We thus infer a different regime of quasi-brittle failure, one that corresponds to a rather prolonged damage evolution (smaller α) owing to damage hardening. Similar variation in the power law exponent describing the divergence in the activity rate of the displacement drops (1 and 1/2) were observed during experiments on specimens of granite and marble [47].

Clearly, quasi-brittle failure has distinct regimes. We consider zones I and III as representative of small and large values of hardening coefficient, respectively and II as the transitional case, as marked in Fig. 1(c) and analyze two data-sets for each zone ($\eta \to 0.05, 0.5, 2.5, 3.0, 15, 25$) at a fixed strength of disorder ($\beta = 0.2$). We compute the distribution of the precursor size S and observe a power law decay in distribution of the precursor size $P(S) \propto S^{-\tau}$ for all data-sets as shown in Fig. 1(e). The value of the exponent for precursors from zones II and III was $\tau \approx 1.3$. For precursors from zone I, a higher value of $\tau \sim 1.45 \pm 0.1$ is obtained. Interestingly, a smaller exponent was also observed during compression experiments on Sidorbe granite [38] on increasing the confining pressure (large damage hardening). Indeed, the power-law statistics of precursors and their divergence as failure is approached seemingly argue for a critical phenomenon interpretation [6–11, 16, 40, 53].

In Mayya *et al.* [28], we untangled these very features of damage evolution resolving scale-free statistics of precursory damage cascades as reminiscent of the avalanches during the depinning of a disordered elastic interface. The power-law divergence of dissipation rate (characterized by exponent $\alpha = 0.5$) is however, shown to emerge from the non-stationary nature of the damage evolution. As the values of damage hardening in zone III ($\eta \to 15, 25$) were comparable to the experimental observations of Mayya *et al.* [28] ($\eta \simeq 40$), we interpret the precursors obtained for large damage hardening as depinning avalanches. Moreover, the failure stress derived using the homogeneous damage evolution considerations was invariant of the strength of disorder [28]. This is in good agreement with the precursors from zone III, as shown in Fig. 1(b). For the case of moderate hardening, we also obtain $\alpha \simeq 0.5$, see Fig. 1(c) but observe a variation in failure stress with disorder. On the other hand, for precursors from zone I, the value of the exponent is significantly larger, $\alpha \sim 0.9$.

Evidence of a different critical transition: To explain the criticality of precursors from zone I and their connection with failure, first we track the value of the damage resistance of the seeds of a cascade $Y_c^{\rm seed}$, the first element

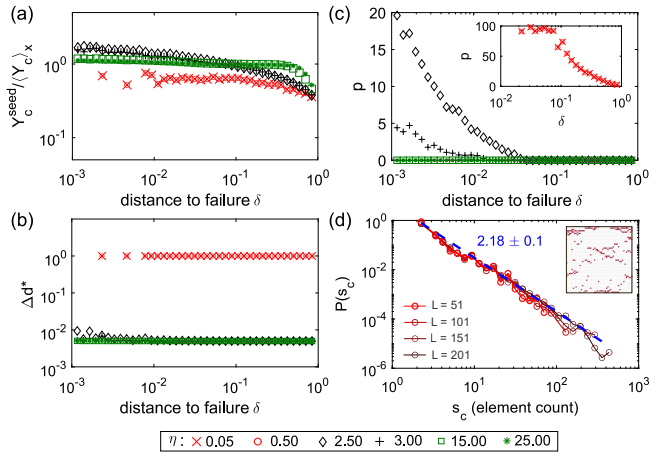

FIG. 2. Variation of (a) the damage resistance of the avalanche seed normalized by the average value, (b) the average incremental damage in the activated elements during the cascade and (c) the concentration of failed elements p with distance to failure δ. The inset of (c) depicts the variations of p with δ for precursors from zone I. (d) Distribution of the size of the clusters in the accumulated damage field when hardening is nearly absent and disorder is moderate ($\beta = 0.2$) for varying specimen size L. Inset: The typical damage field in a system of size $L = 51$ before failure showing clusters of varying size ($\beta = 0.2, \eta = 0.5$).

being damaged during a cascade as shown in Fig. 2(a). Beyond the early stages, damage resistance of the cascade seeds for precursors from zones II and III are comparable to the average value $Y_c^{\text{seed}} < \langle Y_c \rangle_{\text{x}} \geq 1$. Whereas, for zone I, it is shown to be constantly lower than the average value. We now focus on all the elements that are activated during the cascade and determine the variation of the average incremental damage per element in a cascade Δd^* with the distance to failure. We observe the elements from zone I fail completely ($\Delta d^* = 1.0$), in Fig. 2(b). The concentration of failed elements p, i.e., elements with damage level $d(\vec{x}) = 1$ is also shown to increase on approaching failure in Fig. 2(c). In contrast, the material elements activated during the damage cascade resulting in precursors of zone II and III participate only once during the damage cascade, ($\Delta d^* = \delta d_\circ$) as shown in Fig. 2(b) and the the concentration of failed elements p is mostly zero. Indeed, this is consistent with the framework of the depinning transition with a non-positive interaction kernel [54].

The disparities hint at a different universality class for precursors from zone I. Notably, damage spreading is reminiscent of the discrete models of fracture incorporating brittle elements that are reported in literature [21–25, 55, 56]. In particular, it compares well with the case of strong disorder for which percolation-like transition has been discussed. Therefore, we infer the damage spreading in the present case (zone I) also as a percolation-like transition. For validation, we examine the size distribution of the clusters in the damage field prior to failure, see inset of Fig. 2(d). We obtain the scaling relation $P(s_c) \sim s_c^{-\tau_c}$ with $\tau_c = 2.18 \pm 0.1$ as shown in Fig. 2(d). This is in good agreement with the value for percolation in 2D at the threshold, 2.05 [25, 57]. This scaling is further confirmed by the results for larger specimen sizes $L \in [101, 151, 201]$. We note in Fig. 3(c), the size of the largest cluster also increases with specimen size. Also, the value of the exponent describing the divergence of dissipation rate $\alpha \sim 0.9$ obtained for zone I compares well with 0.86 reported in case of a 2D fiber bundle model where the stress release range $\sim r^{-\gamma}$ resembled a global load sharing model for $\gamma \leq 2.2$ [55, 56]. Strikingly, these results provide a critical point description for failure in zone I unlike the approach of an instability for zone II and III [27, 28]. These findings are consistent with the recent discussion in the literature proposing two different universality classes for quasi-brittle failure on the basis of the different exponents of the size distribution [58].

Role of material disorder and elastic interactions: The role of hardening during damage spreading is further illustrated in the top panel of Fig. 3 that depicts the typical damage field at the onset of failure. Increasing the hardening is shown to enhance the homogeneous damage growth. For a better understanding, we recast the discussion in terms of the material disorder and the elastic interactions [59, 60]. Following the incremental damage at the seed, the first element of the cascade (red dot), the redistributions described by the elastic interaction kernel explore different segments of the distribution describing the disorder in damage resistance as shown in the bottom panel of Fig. 3. When damage hardening is

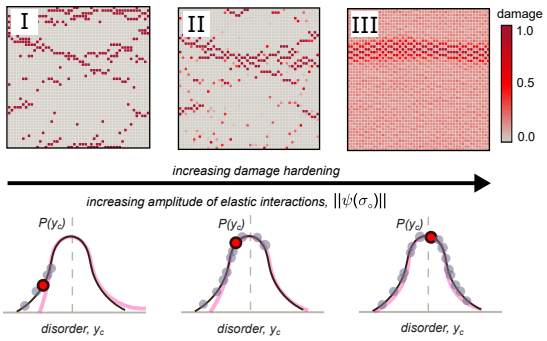

FIG. 3. Top : Typical damage field at onset of failure for zones I ($\eta = 0.5$), II ($\eta = 2.5$) and III ($\eta = 25$) depicting the transition from a heterogeneous to a homogeneous damage evolution that are dominated by material disorder and elastic interactions, respectively. Bottom: Schematic of a damage cascade, close to failure for different cases of hardening. we note the position of the seed of the cascade (red dot) for zone III could be anywhere along the distribution. The redistributions activate different regions (gray dots) of the disorder distribution based on the damage hardening. The change from the original Gaussian distribution in disorder (in black) on approaching failure is shown in magenta [35].

nearly absent, the small amplitude of the redistributions activates only the weaker elements of the disorder distribution. When the disorder is weak, specimen fails catastrophically. However, for strong disorder, the weaker elements are progressively expended and the distribution has a leaner left-branch, close to failure. For large hardening, the redistributions with larger amplitude prevail over the stronger elements resulting in an homogeneous damage evolution. Close to failure, the disorder distribution in this case is then set by the disorder in the incremental damage resistance provided for stabilization of the elements [35]. We thus distinguish the disorder dominated and elastic interactions dominated modes of damage spreading on tuning the hardening. At intermediate levels, damage mostly explores the left branch of the disorder distribution but in contrast to zone I, the elements undergo stable incremental damage.

Quasi-brittleness phase diagram: Seeking to consolidate our findings, we consider a 2D parametric space represented by disorder (abscissa) and hardening coefficient (ordinate) as shown in Fig. 4. To obtain the theoretical bounds of the percolation-like and the depinning type precursors in the diagram, we simplify the stability term of the damage evolution, $\mathcal{K}$ in terms of $Y_c^\circ, E^\circ, d_\circ$ and η, and consider the case of stable incremental damage growth ($d_\circ \to 0$) for the seed of the damage cascades [35]. The damage resistance of the seed is taken as $Y_c^{\text{seed}} = Y_c^\circ(1 - \beta\sqrt{2/\pi})$ where $\beta\sqrt{2/\pi}$ is the mean value of the half-normal distribution describing the elements that are likely to participate in disorder dominated damage spreading process. They constitute the left branch of the original disorder distribution. We then infer the threshold of hardening coefficient η_{th} (in blue) by varying the value of disorder β as

$$\eta_{\text{th}} \simeq 3(1 - \beta\sqrt{2/\pi}). \tag{3}$$

Setting $\beta = 0$ transforms the above equation to homogeneous damage evolution as the damage resistance of the seeds are similar to the average value in the field (see Fig. 2(c)). We obtain $\eta_c \simeq 3$ as the bound for homogeneous damage evolution. These theoretical predictions are in good agreement with the values of the divergence exponent α obtained during the numerical modeling shown in Fig.1(c). For verification, we plot the deviations from the predicted value $|1 - \alpha/\alpha_{\text{pred.}}|$ in Fig. 4 (as diamond markers). The values of $\alpha_{\text{pred.}}$ are 0.9 and 0.5 for small and large hardening, respectively. We find the errors are less than 20% except at strong disorder and is confirmed by the predictions from larger specimen sizes [35]. Lastly, we note that a finite size effect is associated with criticality for $\eta \ll \eta_c$ [25]. Similar inferences when damage hardening is non-trivial will require a detailed analyses and is a part of the on-going studies.

Our findings have interesting implications for quasi-brittle failure. Following the large exponent for the power-law divergence in case of nearly absent hardening (percolation-like scenario), the scaling relations of damage events in experiments may manifest a larger exponent. This is evident in case of the acoustic emissions [61]. The wide-range of Omori law exponents $\alpha_N \sim 0.5 - 1.68$ obtained in literature can be interpreted as emerging from the varying damage hardening: $0.5 < \alpha_N < 1$ corresponding to large damage hardening with damage spreading of the depinning type and $\alpha_N > 1$ as a case of insignificant hardening and the approach to failure is controlled by disorder and reminiscent of the percolation-like transition. The increasing value of the Omori law exponent thus traces the transition from ductile-like to brittle type failure in disordered solids. In summary, we show how material disorder and elastic interactions, through damage hardening organize the transition in brittle to ductile-like failure in disordered solids. Strikingly, this transition manifests in the criticality of precursors as well, reminiscent of the percolation and depinning transitions. Our findings provide a quantitative description of the quasi-brittleness of damage spreading, a topic of strategic value for the design and monitoring of underground structures.

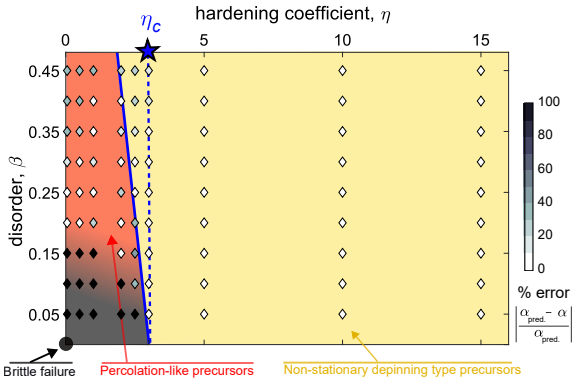

FIG. 4. Phase diagram describing the brittle to quasi-brittle transition during failure of disordered solids with distinct regimes of criticality of failure precursors. The predictions from Eq.(3) for homogeneous damage evolution (dashed line) and depinning type precursors (blue line) are also included. The error in values of the power law divergence exponent α shown in Fig. 1(c) from the theoretical predictions $\alpha_{\text{pred.}}$ are described by the color of the markers.

We thank Laurent Ponson for the helpful discussions and gratefully acknowledge the financial support from Sorbonne Université, CNRS and Satt-Lutech through the project, *Development of a technology of predictive maintenance for materials and structures under compression.*

* ashwijmayya@gmail.com

[1] M. Kachanov, Elastic solids with many cracks: a simple method of analysis, International Journal of Solids and

Structures **23**, 23 (1987).
[2] Z. P. Bažant, Nonlocal damage theory based on micromechanics of crack interactions, Journal of engineering mechanics **120**, 593 (1994).
[3] M. J. Alava, P. K. Nukala, and S. Zapperi, Statistical models of fracture, Advances in Physics **55**, 349 (2006).
[4] D. Lockner, J. Byerlee, V. Kuksenko, A. Ponomarev, and A. Sidorin, Quasi-static fault growth and shear fracture energy in granite, Nature **350**, 39 (1991).
[5] J. Fortin, S. Stanchits, G. Dresen, and Y. Guéguen, Acoustic emission and velocities associated with the formation of compaction bands in sandstone, Journal of Geophysical Research: Solid Earth **111** (2006).
[6] A. Petri, G. Paparo, A. Vespignani, A. Alippi, and M. Costantini, Experimental evidence for critical dynamics in microfracturing processes, Physical Review Letters **73**, 3423 (1994).
[7] A. Garcimartin, A. Guarino, L. Bellon, and S. Ciliberto, Statistical properties of fracture precursors, Physical Review Letters **79**, 3202 (1997).
[8] S. Deschanel, L. Vanel, G. Vigier, N. Godin, and S. Ciliberto, Statistical properties of microcracking in polyurethane foams under tensile test, influence of temperature and density, Int. J. Frac. **140**, 87 (2006).
[9] J. Davidsen, S. Stanchits, and G. Dresen, Scaling and universality in rock fracture, Physical review letters **98**, 125502 (2007).
[10] J. Rosti, J. Koivisto, and M. J. Alava, Statistics of acoustic emission in paper fracture: precursors and criticality, Journal of Statistical Mechanics: Theory and Experiment **2010**, P02016 (2010).
[11] J. Baró, Á. Corral, X. Illa, A. Planes, E. K. Salje, W. Schranz, D. E. Soto-Parra, and E. Vives, Statistical similarity between the compression of a porous material and earthquakes, Physical review letters **110**, 088702 (2013).
[12] G. F. Nataf, P. O. Castillo-Villa, J. Baró, X. Illa, E. Vives, A. Planes, and E. K. Salje, Avalanches in compressed porous si o2-based materials, Physical Review E **90**, 022405 (2014).
[13] S.-T. Tsai, L.-M. Wang, P. Huang, Z. Yang, C.-D. Chang, and T.-M. Hong, Acoustic emission from breaking a bamboo chopstick, Physical Review Letters **116**, 035501 (2016).
[14] J. Baró, A. Planes, E. K. Salje, and E. Vives, Fracking and labquakes, Philosophical Magazine **96**, 3686 (2016).
[15] J. Davidsen, T. Goebel, G. Kwiatek, S. Stanchits, J. Baró, and G. Dresen, What controls the presence and characteristics of aftershocks in rock fracture in the lab?, Journal of Geophysical Research: Solid Earth **126**, e2021JB022539 (2021).
[16] C.-C. Vu, D. Amitrano, O. Plé, and J. Weiss, Compressive failure as a critical transition: Experimental evidence and mapping onto the universality class of depinning, Phys. Rev. Lett. **122**, 015502 (2019).
[17] L. Wang, S. Cao, X. Jiang, and E. K. Salje, Cracking of human teeth: An avalanche and acoustic emission study, Journal of the Mechanical Behavior of Biomedical Materials **122**, 104666 (2021).
[18] We consider the scaling relation associated with the activity rate of events between two successive large signals [11] as also describing the approach to failure.
[19] D. Triantis and S. K. Kourkoulis, An alternative approach for representing the data provided by the acoustic emission technique, Rock Mechanics and Rock Engineering **51**, 2433 (2018).
[20] D. Sornette, Sweeping of an instability: an alternative to self-organized criticality to get power laws without parameter tuning, J. Phys. I **4**, 209 (1994).
[21] S. Zapperi, P. Ray, H. E. Stanley, and A. Vespignani, First-order transition in the breakdown of disordered media, Physical review letters **78**, 1408 (1997).
[22] H. B. da Rocha and L. Truskinovsky, Rigidity-controlled crossover: From spinodal to critical failure, Physical Review Letters **124**, 015501 (2020).
[23] S. Roux, A. Hansen, H. Herrmann, and E. Guyon, Rupture of heterogeneous media in the limit of infinite disorder, Journal of statistical physics **52**, 237 (1988).
[24] Y. Moreno, J. Gomez, and A. Pacheco, Fracture and second-order phase transitions, Physical review letters **85**, 2865 (2000).
[25] A. Shekhawat, S. Zapperi, and J. P. Sethna, From damage percolation to crack nucleation through finite size criticality, Physical review letters **110**, 185505 (2013).
[26] S. Biswas, S. Roy, and P. Ray, Nucleation versus percolation: Scaling criterion for failure in disordered solids, Physical Review E **91**, 050105 (2015).
[27] E. Berthier, A. Mayya, and L. Ponson, Damage spreading in quasi-brittle disordered solids: Ii. what the statistics of precursors teach us about compressive failure, Journal of the Mechanics and Physics of Solids **162**, 104826 (2022).
[28] A. Mayya, E. Berthier, and L. Ponson, How criticality meets bifurcation in compressive failure of disordered solids, HAL archive **hal-03518512** (2022).
[29] A. L. Barabási and H. E. Stanley, *Fractal concepts in surface growth* (Cambridge University Press, 1995).
[30] O. Narayan and D. S. Fisher, Threshold critical dynamics of driven interfaces in random media, Physical Review B **48**, 7030 (1993).
[31] A. Mayya, E. Berthier, and L. Ponson, Procédé et dispositif d'analyse d'une structure. french patent application fr2002824 (2020).
[32] D. Kumar, A. Banerjee, and R. Rajesh, Interplay between disorder and hardening during tensile fracture of a quasi-brittle solid, Proceedings of the Royal Society A **478**, 20210934 (2022).
[33] E. Berthier, V. Démery, and L. Ponson, Damage spreading in quasi-brittle disordered solids: I. localization and failure, Journal of the Mechanics and Physics of Solids **102**, 101 (2017).
[34] V. Dansereau, V. Démery, E. Berthier, J. Weiss, and L. Ponson, Collective damage growth controls fault orientation in quasibrittle compressive failure, Physical review letters **122**, 085501 (2019).
[35] A. Mayya, Supplementary information : On the transitions in quasi-brittle failure of disordered solids" (2022).
[36] K. J. Wiese, Theory and experiments for disordered elastic manifolds, depinning, avalanches, and sandpiles, arXiv preprint arXiv:2102.01215 (2021).
[37] D. Amitrano, J.-R. Grasso, and D. Hantz, From diffuse to localised damage through elastic interaction, Geophysical research letters **26**, 2109 (1999).
[38] D. Amitrano, Brittle-ductile transition and associated seismicity: Experimental and numerical studies and relationship with the b value, Journal of Geophysical Research: Solid Earth **108** (2003).
[39] R. Ince, A. Arslan, and B. Karihaloo, Lattice modelling

of size effect in concrete strength, Engineering Fracture Mechanics **70**, 2307 (2003).
[40] L. Girard, D. Amitrano, and J. Weiss, Failure as a critical phenomenon in a progressive damage model, Journal of Statistical Mechanics: Theory and Experiment **2010**, P01013 (2010).
[41] G.-F. Zhao, J. Fang, and J. Zhao, A 3d distinct lattice spring model for elasticity and dynamic failure, International Journal for Numerical and Analytical Methods in Geomechanics **35**, 859 (2011).
[42] L. Girard, J. Weiss, and D. Amitrano, Damage-cluster distributions and size effect on strength in compressive failure, Physical review letters **108**, 225502 (2012).
[43] M. Kiyoo, Pressure dependence of rock strength and transition from brittle fracture to ductile flow, Bulletin of the Earthquake Research Institute **44**, 215 (1966).
[44] H. Horii and S. Nemat-Nasser, Brittle failure in compression: splitting faulting and brittle-ductile transition, Philosophical Transactions of the Royal Society of London. Series A, Mathematical and Physical Sciences **319**, 337 (1986).
[45] B. Evans, J. T. Fredrich, and T.-F. Wong, The brittle-ductile transition in rocks: Recent experimental and theoretical progress, The brittle-ductile transition in rocks **56**, 1 (1990).
[46] C. E. Renshaw and E. M. Schulson, Universal behaviour in compressive failure of brittle materials, Nature **412**, 897 (2001).
[47] J. Xue, S. Hao, J. Wang, F. Ke, C. Lu, and Y. Bai, The changeable power law singularity and its application to prediction of catastrophic rupture in uniaxial compressive tests of geomedia, Journal of Geophysical Research: Solid Earth **123**, 2645 (2018).
[48] A. Cartwright-Taylor, I. G. Main, I. B. Butler, F. Fusseis, M. Flynn, and A. King, Catastrophic failure: How and when? insights from 4-d in situ x-ray microtomography, Journal of Geophysical Research: Solid Earth **125**, e2020JB019642 (2020).
[49] J. Escartín, G. Hirth, and B. Evans, Nondilatant brittle deformation of serpentinites: Implications for mohr-coulomb theory and the strength of faults, Journal of Geophysical Research: Solid Earth **102**, 2897 (1997).
[50] O. Katz and Z. Reches, Microfracturing, damage, and failure of brittle granites, Journal of Geophysical Research: Solid Earth **109** (2004).
[51] T.-f. Wong and P. Baud, The brittle-ductile transition in porous rock: A review, Journal of Structural Geology **44**, 25 (2012).
[52] G. Hirth and J. Tullis, The brittle-plastic transition in experimentally deformed quartz aggregates, Journal of Geophysical Research: Solid Earth **99**, 11731 (1994).
[53] J. Weiss, L. Girard, F. Gimbert, D. Amitrano, and D. Vandembroucq, (finite) statistical size effects on compressive strength, Proceedings of the National Academy of Sciences **111**, 6231 (2014).
[54] J. Lin, T. Gueudré, A. Rosso, and M. Wyart, Criticality in the approach to failure in amorphous solids, Physical Review Letters **115**, 168001 (2015).
[55] R. C. Hidalgo, Y. Moreno, F. Kun, and H. J. Herrmann, Fracture model with variable range of interaction, Physical review E **65**, 046148 (2002).
[56] O. E. Yewande, Y. Moreno, F. Kun, R. C. Hidalgo, and H. J. Herrmann, Time evolution of damage under variable ranges of load transfer, Physical Review E **68**, 026116 (2003).
[57] R. M. Ziff, Correction-to-scaling exponent for two-dimensional percolation, Physical Review E **83**, 020107 (2011).
[58] Y. Xu, A. G. Borrego, A. Planes, X. Ding, and E. Vives, Criticality in failure under compression: Acoustic emission study of coal and charcoal with different microstructures, Physical Review E **99**, 033001 (2019).
[59] S. Roy, S. Biswas, and P. Ray, Modes of failure in disordered solids, Physical Review E **96**, 063003 (2017).
[60] S. Sinha, S. Roy, and A. Hansen, Crack localization and the interplay between stress enhancement and thermal noise, Physica A: Statistical Mechanics and its Applications **569**, 125782 (2021).
[61] We consider the individual acoustic signals as representative of the localized damage events - their activity rate follows a power-law divergence on approaching failure. In contrast, the activity rate of the spatio-temporally distributed damage cascades is a constant. Still, we expect the overall increase in energy dissipation rate during the damage spreading process that results in a larger exponent α to also manifest a larger exponent for the activity rate of the acoustic signals α_N.

SUPPLEMENTARY INFORMATION

The collective nature of damage spreading

A characteristic aspect of the failure of brittle disordered solids is the intermittently occurring precursory damage bursts. The macroscopic response during a force (displacement) controlled loading is marked by force plateaus (load drops) corresponding to the force (displacement) at which damage $d(\vec{x})$ evolves in parts of the specimen. These failure precursors are described by robust scaling relations and are understood as cascades of incremental damage as shown in Fig. 1(a). They result from the co-action of the material disorder and the elastic interactions in the damage field [1, 2]. The quasi-static increments of the loading amplitude (here, applied stress $\sigma_\circ$) activates one of the material

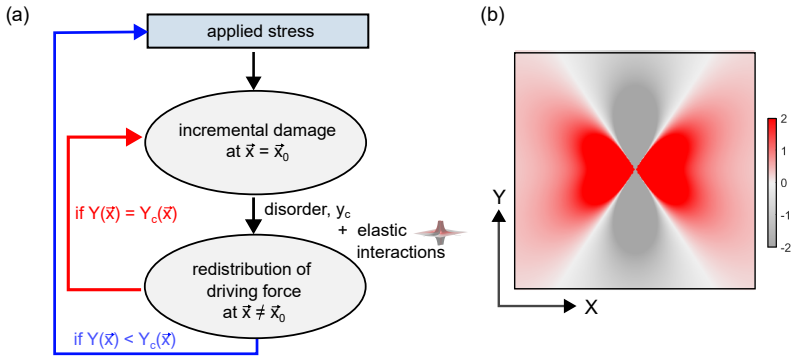

FIG. 1. (a) Schematic of the mechanism of damage evolution in disordered solids. (b) The functional form of the kernel $\psi(d_\circ)$ describing the elastic interactions in the damage field for the case of uniaxial compression in 2D.

elements located in $\vec{x} = \vec{x}_0$ following the damage criterion [2, 3] that compares the loading dependent damage driving force $Y[d(\vec{x}), \sigma_\circ]$ with the damage resistance $Y_c[\vec{x}, d(\vec{x})]$, a material property. The local damage level is updated as $d(\vec{x}_0) = d(\vec{x}_0) + \delta d_\circ$. The element is then locally stabilized as $\mathcal{K} = \frac{\partial(Y_{c\circ} - Y_\circ)}{d_\circ} > 0$ during the precursory damage accumulation. The local softening results in a change of the damage driving force of the neighbors and is given by $\psi(\vec{x} - \vec{x}_0)\delta d_\circ$. It corresponds to the redistributions of the elastic energy in the damage field and is defined by the long-range interaction kernel $\psi(d_\circ)$. As a result, other elements may be activated triggering a cascade that stops when the disorder in damage resistance prevails over the redistributions. The interaction kernel for the present work is derived using the method described in Dansereau *et al.* [2] and writes as

$$\psi(d_\circ) = \left[\frac{E'(d_\circ)^2}{E(d_\circ)^3}\right](1-\nu^2)\sigma_{ext}^2\left[\frac{x^4 - 3y^4 + 6x^2y^2}{4\pi(x^2+y^2)^3}\right] \rightarrow ||\psi||\left[\frac{\cos^4\theta - 3\sin^4\theta + 6\cos^2\theta\sin^2\theta}{4\pi r^6}\right]. \quad (4)$$

The functional form of kernel with quadru-polar symmetry is shown in Fig. 1(b). In Dansereau *et al.* [2], it was shown that the the orientation of the maximum lobes of the kernel control the orientation of the localization band. Importantly, this prediction is independent of the damage hardening coefficient as observed in Fig. 3(a) of the main article.

Individual roles of disorder and damage hardening

The macroscopic response obtained for a fixed hardening coefficient and varying disorder is shown in different panels of Fig. 2. We note the material disorder β plays an important role when damage hardening is nearly absent. Failure takes place at progressively lower value of stress and a higher value of failure strain. The transformation in damage spreading is evident on increasing the hardening coefficient η. For large hardening coefficient, the value of critical stress and strain do not vary with disorder. On the other hand, when we compare the three panels and fix the strength of disorder, the damage hardening is shown to result in an enhanced load bearing capacity.

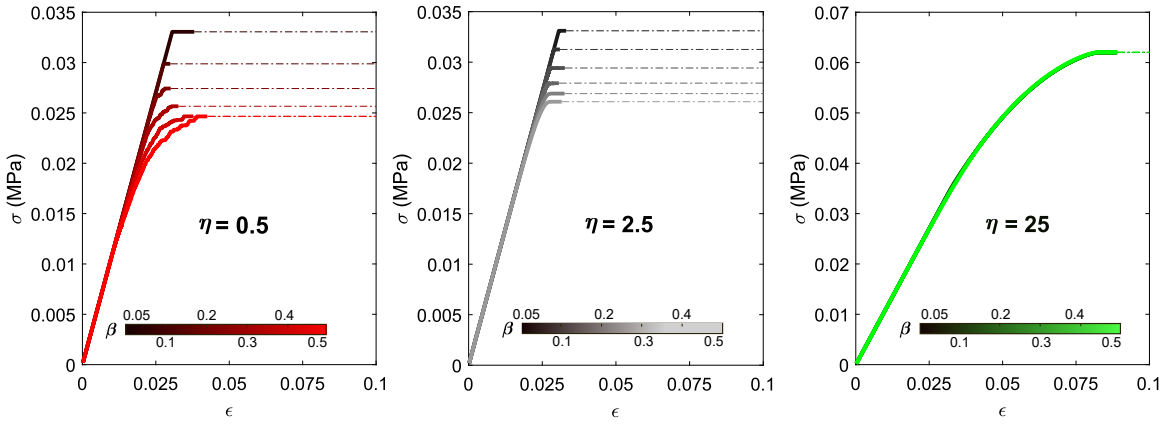

FIG. 2. The typical stress-strain response obtained for a given hardening coefficient and varying strength of disorder in each panel. Higher disorder is shown in darker colors. The damage hardening of the data-sets increases from left to right.

Evolution of disorder in damage resistance

We track the disorder in the field of damage resistance during the damage spreading to further understand its role in relation to the damage hardening. The distribution of the field of damage resistance normalized by the average value is plotted at different distances to failure δ and shown in Fig.3. When hardening is nearly absent, the left branch of the distribution is shown to progressively become leaner with the weaker elements being expended during damage spreading. Consequently, these elements have a rather large damage resistance that appear distinctly on the right branch. Similar features are observed when hardening is moderate. However, the partial damage of the weaker elements results in marginal increase of the damage resistance and therefore a second peak on the right branch is not observed. We note that the right branch did not get fatter in both cases implying the that the strong elements did not participate in damage spreading.

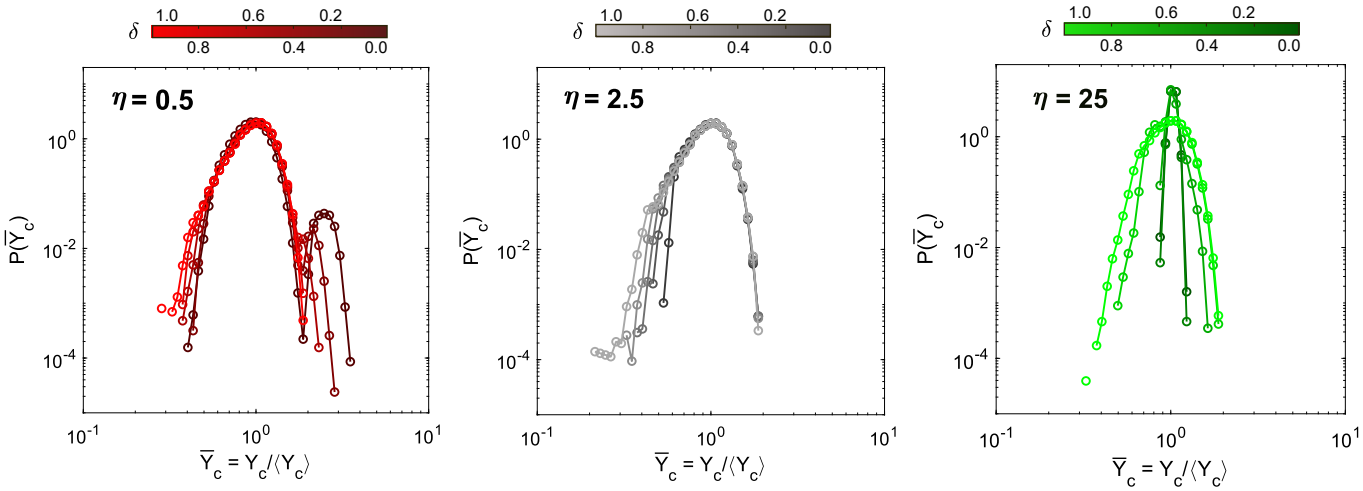

FIG. 3. Distribution of the damage resistance normalized by the mean value $\overline{Y_c} = Y_c/\langle Y_c\rangle$ at fixed damage hardening at different distances to failure. The plots are darker on approaching failure ($\delta = 0$). The damage hardening of the data-sets increases from left to right.

In contrast, when the hardening coefficient was large, the distribution becomes leaner approaching the average value, $\mathcal{N}(Y_{co}, 0)$ from the original disordered field, $\mathcal{N}(Y_{co}, 0.2)$. The narrow distribution close to failure rather corresponds to the distribution of the incremental damage resistance that stabilizes the element undergoing damage.

Threshold hardening for stable damage evolution

As the failure strength and the manner of damage spreading are clearly shown to vary with the hardening coefficient, we expect a threshold value for hardening at which the elastic interactions dominate over material disorder. Taking inspiration from the panels on the right-side in Figs. 2 and 3, we first consider the case of homogeneous damage evolution. The stability of the damage evolution given by[3],

$$\mathcal{K} \rightarrow \frac{\partial(Y_{c\circ} - Y_\circ)}{\partial d_\circ} \geq 0, \tag{5}$$

where we have also considered the limiting case of the stability criterion $\mathcal{K} = 0$. $Y_{c\circ}, Y_\circ$ are the average values taken to represent the damage resistance and damage driving force of the elements being activated during the homogeneous damage evolution, respectively. Following the damage hardening rule, $Y_{c\circ} = Y_c^\circ(1 + \eta d_\circ)$ the first term of the above equation is given by

$$\frac{\partial Y_{c\circ}}{\partial d_\circ} = Y_c^\circ \eta, \tag{6}$$

where Y_c° is the characteristic damage resistance of the undamaged material and η is the hardening coefficient. As the damage driving force is the rate of elastic energy release with incremental damage $\frac{d}{dd_\circ}\left(\frac{(1-\nu^2)\sigma_\circ^2}{2E_\circ}\right)$, the second term of the Eq. (5) writes as

$$\frac{\partial Y_\circ}{\partial d_\circ} = \frac{(1-\nu^2)\sigma_\circ^2}{2}\frac{d}{dd_\circ}\left(\frac{-E'_\circ}{E_\circ^2}\right) \rightarrow \frac{3(1-\nu^2)\sigma_\circ^2}{E^\circ(1-d_\circ)^4}, \tag{7}$$

where $E_\circ = E^\circ(1-d_\circ)^2$ and $E'_\circ = -2E^\circ(1-d_\circ)$. From the equilibrium condition $Y_\circ(d_\circ) = Y_{c\circ}(d_\circ)$, we derive $\sigma_\circ^2 = \frac{Y_{c\circ}E^\circ(1-d_\circ)^3}{(1-\nu^2)}$. Using this relation of $\sigma_\circ$ and $Y_{c\circ}$ in the above equation, the second term of Eq. (5) writes as

$$\frac{\partial Y_\circ}{\partial d_\circ} = \frac{3Y_c^\circ(1+\eta d_\circ)}{(1-d_\circ)}. \tag{8}$$

Using Eqs. (5),(6) and (8), the relation between the hardening coefficient η and the mean damage level $d_\circ$ is then obtained as

$$\eta \geq \frac{3(1+\eta d_\circ)}{(1-d_\circ)}. \tag{9}$$

For the incremental damage to be stable we take $d_\circ \rightarrow 0$ and consider the equality in the above relation to obtain the threshold value $\eta_c \simeq 3$ for the case of stable homogeneous damage evolution. For $\eta < \eta_c$, the damage spreading is dominated by the strength of the material disorder β. Close to η_c, one expects a transition where the incremental damage of the elements is stable. The equilibrium in this case is satisfied by the damage driving force balanced by the damage resistance of the weaker elements that are activated at the start of the damage cascade, $Y_\circ(d_\circ) = Y_{c\circ}^{\text{seed}}(d_\circ)$. Considering the left-branch of the original normal distribution as the half-normal distribution of the seeds of the damage cascades, the value of $Y_{c\circ} \rightarrow Y_{c\circ}(1-\beta\sqrt{2/\pi})$. Thus, for the disorder dominated damage spreading ($\eta < \eta_c$), Eq. (8) writes as

$$\frac{\partial Y_\circ}{\partial d_\circ} = \frac{3Y_c^\circ(1+\eta d_\circ)}{(1-d_\circ)}(1-\beta\sqrt{2/\pi}) \tag{10}$$

Following Eqs.(5), (6) and (10), the hardening coefficient η writes as

$$\eta \geq \frac{3(1-\beta\sqrt{2/\pi})}{1-d_\circ[1+3(1-\beta\sqrt{2/\pi})]}. \tag{11}$$

As $d_\circ \rightarrow \delta d_\circ \sim 0$, we obtain the threshold value of damage hardening to ensure stable incremental damage as

$$\eta_{\text{th}} \simeq 3(1-\beta\sqrt{2/\pi}). \tag{12}$$

Setting the value of strength of disorder $\beta = 0$ to rationalize the effect of elastic interactions prevailing over the material disorder i.e., a homogeneous damage evolution, we recover $\eta_c \simeq 3$. The above relation describes the boundary of the quasi-brittleness diagram where the precursors diverge on approaching failure with an exponent $\alpha \simeq 0.5$. Although the disorder in the damage field grows when $\eta < \eta_c$ during the damage spreading, in presence of strong disorder, it resembles the early stages of the transient roughening process of the depinning framework. The theoretical bounds are shown to be in good agreement with the results from numerical modeling in Fig. 3(b) of the main article.

Effect of specimen size on the power-law divergence

To verify the theoretical predictions of varying hardening threshold η_{th} with the strength of disorder β, we run simulations for $\eta \in [2, 3]$ for different system sizes. The value of the exponents characterizing the power law divergence on approach to failure and their deviation from the predictions are shown in Fig.4. In absence of a power law scaling of precursors on approaching failure, we infer the failure as brittle type. On increasing the system size, the limits for the brittle failure ($\beta \leq 0.10$)is shown to marginally increase. Even at $\eta = 3$, the limit for the homogeneous damage evolution, the error in divergence exponent increases with system size. At moderate disorder, the predictions of hardening threshold (blue line) from the theory are in good agreement with the divergence exponents and the errors are generally less than 15% . When the disorder is strong, we observe larger deviations from theory ($\sim 20\%$) that are also enhanced with increasing system size ($> 20\%$).

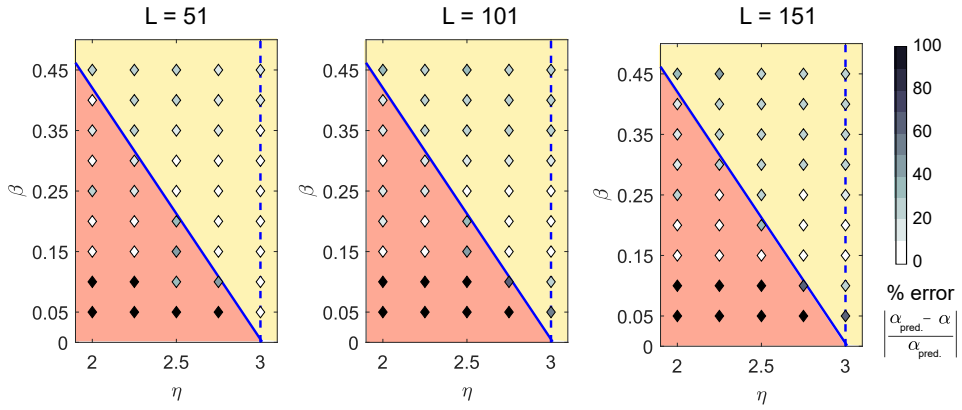

FIG. 4. The map of divergence exponent obtained for different cases of disorder β and hardening coefficient η. The markers correspond to the predictions following the theoretical bounds given by Eq. (12) and their color describes the absolute error. This allows for a comparison of the prediction of hardening threshold (blue line) for varying strength of disorder with the divergence exponent α for three cases of system size L.

* ashwijmayya@gmail.com

[1] J. Weiss, L. Girard, F. Gimbert, D. Amitrano, and D. Vandembroucq, (finite) statistical size effects on compressive strength, Proceedings of the National Academy of Sciences **111**, 6231 (2014).

[2] V. Dansereau, V. Démery, E. Berthier, J. Weiss, and L. Ponson, Collective damage growth controls fault orientation in quasibrittle compressive failure, Physical review letters **122**, 085501 (2019).

[3] E. Berthier, V. Démery, and L. Ponson, Damage spreading in quasi-brittle disordered solids: I. localization and failure, Journal of the Mechanics and Physics of Solids **102**, 101 (2017).